Modification of Network and Pore Dimensionality in Metal-Organic Frameworks Containing a Secondary Phosphine Functionality

*Andrey A. Bezrukov, Karl W. Törnroos and Pascal D. C. Dietzel**

Department of Chemistry, University of Bergen, P.O. Box 7803, N-5020 Bergen, Norway

ABSTRACT. Three new metal-organic frameworks containing a triphenylphosphine moiety, namely $[Zn_3(tpp)_2(DMF)_2]\cdot n$DMF (**1**), $[Zn_3(tpp)_2(4,4'\text{-bipy})_2]\cdot n$DMF (**2**) and $[Zn_3(tpp)_2(3,3'\text{-bipy})]\cdot n$DMF (**3**), were synthesized using 4,4',4''-phosphanetriyltribenzoic acid (H_3tpp) as a tritopic tridentate linker. The absence or presence of additional N-donor linker molecules in the reaction mixture directed the formation of (3,6)-c layered, (3,8)-c pillared layered or (3,4,6)-c frameworks. Compound **1** is composed of a trinuclear zinc secondary building unit (SBU) and the tpp^{3-} anion arranged in a layered (3,6)-c network with **kgd** topology. There are guest DMF molecules coordinated to the terminal Zn atoms of the trinuclear inorganic SBU. The addition of the neutral N-donor molecules 3,3'-bipyridine (3,3'-bipy) and 4,4'-bipyridine (4,4'-bipy) as second organic linker molecule lead to an increase of dimensionality of the networks. Compound **2** is a (3,4,6)-nodal three-dimensional MOF. Its structure consists of two equivalent interpenetrated nets with the point symbol $(5^2\cdot6^4)(5^2\cdot6)_2(5^4\cdot6^6\cdot7^2\cdot8\cdot9^2)$ with solvent filled pockets. The free electron pair of phosphorus atom of the triphenylphosphine moiety is pointing towards the 0-dimensional pores.

The structure of **3** can be described as layers of **1** which are connected by additional 3,3'-bipyridine as pillar into a three-dimensional (3,8)-c network with the point symbol $(4^3)_2(4^6{\cdot}6^{18}{\cdot}8^4)$. The non-interpenetrated structure of **3** contains a solvent filled three-dimensional pore system. All three materials exhibit uptake of CO_2 at 195 K after removal of the guest DMF molecules. It is particularly surprising for **2**, with its 0-dimensional pores in the single crystal structure and absence of N_2 adsorption at 77 K. **3** showed a large gate opening effect for CO_2 adsorption at 195 K.

INTRODUCTION

Metal-Organic Frameworks (MOFs) are coordination networks with solvent filled pores built from organic linker and metal cations or clusters. Multifunctional organic linkers that contain donor functional groups[1] that are not involved in the coordination to the metal are of particular interest because they can act as anchor for grafting catalytically active transition metals into the pores of the MOF.[2-5] A functional group that is eminently useful in this respect is the phosphine functional group. Its presence enables the immobilization of organometallic complexes widely used in catalytic reactions, such as C–C couplings, olefin metathesis and oligomerization, hydrogenation and hydroformylation.[6] Incorporation of phosphine functional groups into porous materials other than MOFs has been achieved, for example in porous polymers[7-9], covalent-organic frameworks[10-13] and inorganic supports as mesoporous silica's.[14-16] For the incorporation in MOFs, it is a natural approach is to use a suitable derivative of triphenyl phosphine, such as the tritopic 4,4',4''-phosphanetriyltribenzoic acid (H_3tpp). Humphrey *et al*. has reported three Zn-tpp frameworks (PCM-1, PCM-2 and PCM-3),[17] all of which were two-dimensional coordination polymers with honeycomb-like networks. A three-dimensional permanently porous tpp^{3-} based MOF was obtained with calcium (PCM-10).[18] An Au(I) complex was grafted to the available P-site and the

material was used for 1-hexene/n-hexane separation. In addition, the adsorption properties of the material towards different gases were tuned by using different post-synthetic modifications of the phosphine site.[19] Bokhoven *et al.* prepared a Zr-based coordination polymer with tpp^{3-} onto which an Au(I) complex was grafted.[20] The resulting material catalyzed hydration and cyclization reactions. Recently, Wenbin Lin *et al.* immobilized Rh and Ir based organometallic complexes in a Zr-MOF synthesized using an elongated version of the H_3tpp tritopic linker. The material showed activity in a broad scope of catalytic reactions.[21] A related approach is the incorporation of chelating ligands into the framework, which is expected to result in more stable complexes and lower metal leakage than for monodentate complexes. For instance, Humphrey incorporated a linker containing bis(phosphine)MCl_2 complexes in the framework.[22] Wenbin Lin *et al*. used a long linear BINAP-based linker to introduce chiral bisphosphine moiety into the MOF with UiO topology.[23] The resulting MOF was functionalized further with complexes with Ru and Rh and tested in a broad range of asymmetric catalytic reactions.

Another fruitful approach for preparation of MOFs with known topologies and available anchor sites is the use of derivatives of linear linkers, e.g. terephthalic acid carrying the phosphine functionality on a side-chain. Kapteijn *et al*. used post-synthetic chloromethylation of MIL-101(Cr) with consecutive chlorine substitution to achieve introduction of diphenylphosphine into the structure.[24] Bokhoven *et al.* used the isoreticular approach to build MOF-5 and MIL-101 analogs with triphenyl phosphine-derivatized terephthalic acid.[25] The same group also used the 4,4′-dicarboxylic acid with triphenylphosphine functionality as linker in synthesis of mixed-linker frameworks with IRMOF-9 topology and tested the MOF as a catalyst in catalytic and stoichiometric reactions.[26]

Herein, we present three triphenylphosphine based MOFs that were synthesized from 4,4',4''-phosphanetriyltribenzoic acid (H_3tpp) (Scheme 1). By adding neutral 4,4’-bipyridine (4,4’-bipy)

and 3,3'-bipyridine (3,3'-bipy) linkers in one-pot synthesis it was possible to direct the synthesis towards (3,6)-connected layered (**1**), (3,8)-connected pillared layered (**3**) or (3,4,6)-connected (**2**) frameworks. The layers in the pillared-layered structure **3** are equivalent to the layers found in **1**, while **2** has a completely different arrangement of structure building units. Frameworks **1-3** have solvent filled pores and desolvated materials display CO_2 adsorption.

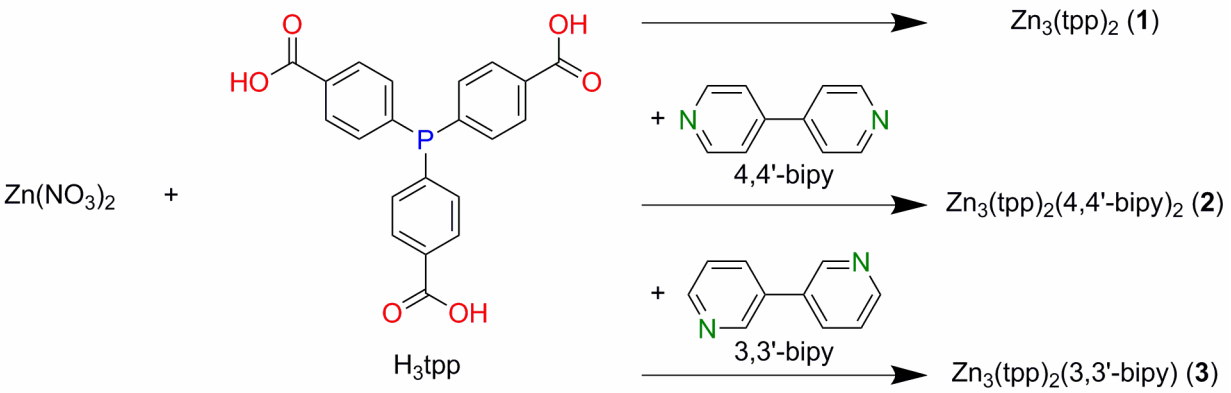

Scheme 1. Syntheses of compounds **1-3**.

EXPERIMENTAL SECTION

Materials

All chemicals, reagents and solvents were purchased from Sigma-Aldrich and used as received without further purification. Synthesis of the MOFs was performed under inert conditions in order to prevent oxidation of P(III) to P(V). Manipulations under inert atmosphere were performed using Schlenk technique or in a glove box (MBRAUN). Water- and oxygen-free tetrahydrofuran (THF) and dichloromethane were collected using a solvent purification system (MBRAUN SPS-800). Dimethylformamide (DMF) was deaerated using the freeze-pump-thaw procedure. Water, hydrochloric acid solution and chloroform were deaerated by purging with Ar. Gases used in physisorption experiments were of 99.9995%, or higher, purity and were purchased from Yara

Praxair. Infrared (IR) spectra were recorded on a Nicolet 380 FTIR spectrometer, equipped with an ATR unit, in the spectral range 4000-650 cm^{-1} at room temperature.

Synthesis of 4,4',4''-phosphanetriyltribenzoic acid (H_3tpp). 4,4',4"-phosphanetriyltribenzoic acid (H_3tpp) was synthesised based on procedures adapted from literature (experimental details are given in the Supplementary Information). The first two steps were performed using a scaled up version of the procedure reported by Amengual *et al.*[27] The third step was performed using the procedure reported by Humphrey *et al.*[17].

Synthesis of [Zn_3(tpp)$_2$(DMF)$_2$]·*n*DMF (1). Single crystals for crystal structure determination were originally obtained using the following procedure: zinc(II) nitrate hexahydrate (45 mg, 0.15 mmol) and H_3tpp (39 mg, 0.1 mmol) were placed into a glass culture tube with screw cap (Schott, ~6 mL). The open tube was placed in a larger Schlenk flask. The atmosphere in the flask was exchanged to Ar and the following operations were performed under Ar flow. Deaerated DMF (3 mL) was added to the mixture of solids. The tube was closed with a cap and taken out of the larger Schlenk flask. The reaction mixture was sonicated for half an hour, during which complete dissolution of the reactants was observed. The tube was then placed in an oven pre-heated to 383 K. The tube was taken out after 2 days and allowed to cool to room temperature. The solid product was filtered and washed with DMF. For further experiments, the synthesis was scaled up by the factor of 2 by increasing the concentration and the reaction temperature was changed to 363 K while other parameters were the same. Yield: 89 mg (70 %, based on the formula [Zn_3(tpp)$_2$(DMF)$_2$]·2DMF). ν_{max}/cm^{-1}: 2929, 1675, 1662, 1595, 1547, 1493, 1407, 1386, 1370, 1343, 1306, 1275, 1253, 1184, 1133, 1115, 1088, 1061, 1017, 858, 844, 775, 770, 723, 717, 699, 668, 658. The observed powder X-ray diffraction pattern of compound **1** corresponds with the pattern calculated from the single crystal structure (Figure S1).

Synthesis of [$Zn_3(tpp)_2(4,4'\text{-bipy})_2$]·*n*DMF (2). Zinc(II) nitrate hexahydrate (89 mg, 0.3 mmol), H_3tpp (79 mg, 0.2 mmol) and 4,4'-bipyridine (31 mg, 0.2 mmol) were placed into a glass culture tube with screw cap (Schott, ~6 mL). The open tube was placed in a larger Schlenk flask. The atmosphere in the flask was exchanged to Ar and the following operations were performed under Ar flow. Deaerated DMF (3 mL) was added to the mixture of solids. The tube was closed with a cap and taken out of the larger Schlenk flask. The reaction mixture was sonicated for half an hour, during which complete dissolution of the reactants was observed. The tube was then placed in an oven pre-heated to 363 K. The tube was taken out after 1 day and allowed to cool to room temperature. The solid product was filtered and washed with DMF. Yield: 128 mg (89 % based on the formula $[Zn_3(tpp)_2(4,4'\text{-bipy})_2]\cdot 2DMF$). ν_{max}/cm^{-1}: 3051, 2916, 1676, 1635, 1611, 1593, 1550, 1492, 1408, 1392, 1301, 1274, 1257, 1222, 1180, 1136, 1085, 1075, 1048, 1014, 864, 843, 815, 773, 737, 721, 699, 658. The observed powder X-ray diffraction pattern of compound **2** corresponds with the one calculated from the single crystal structure (Figure S3).

Synthesis of [$Zn_3(tpp)_2(3,3'\text{-bipy})$]·*n*DMF (3). Zinc(II) nitrate hexahydrate (89 mg, 0.3 mmol), H_3tpp (79 mg, 0.2 mmol) and 3,3'-bipyridine (13.5 μL, 0.1 mmol) were placed into the glass culture tube (Schott, ~20 mL). The open tube was placed in a larger Schlenk flask. The atmosphere in the flask was exchanged to Ar and the following operations were performed under Ar flow. Deaerated DMF (5 mL) was added to the mixture of solids. The tube was closed with a cap and taken out of the larger Schlenk flask. The reaction mixture was sonicated for half an hour, during which complete dissolution of the reactants was observed. The tube was then placed in an oven pre-heated to 363 K. The tube was taken out after 3 days and allowed to cool to room temperature. The solid product was filtered and washed with DMF. Yield 153 mg (93 % based on the formula $[Zn_3(tpp)_2(3,3'\text{-bipy})]\cdot 7DMF$). ν_{max}/cm^{-1}: 2926, 2854, 1668, 1595, 1546, 1493, 1472, 1405, 1384,

1339, 1306, 1255, 1182, 1134, 1088, 1063, 1043, 1018, 862, 845, 802, 772, 718, 701, 659. The observed powder X-ray diffraction pattern of compound **3** and with the pattern calculated from the single crystal structure are compared in Figure S4a. The purity of the bulk phase was confirmed by Pawley fitting of the bulk powder sample (Figure S4b).

Single-crystal structural determination. Suitable crystals for diffraction experiments were mounted in a minimum amount of Parabar 10312 oil (Hampton Research) in a nylon loop. Intensity data for **1** was collected at beamline BM01A of the Swiss-Norwegian Beamlines (SNBL) at ESRF using a custom made one-axis diffractometer with PILATUS 2M detector.[28] The data processing was performed using the CrysAlisPro software.[29] Intensity data for **2** and **3** was collected with a Bruker AXS TXS rotating anode system with an APEX II Pt^{135} CCD detector using graphite-monochromated Mo *Kα* radiation. Data collection and data processing were done using APEX2,[30] SAINT,[31] and SADABS[32] version 2008/1. The structure solution and final model refinement for all structures were performed using SHELXS[33] version 2013/1 or SHELXT[34] version 2014/4 and SHELXL[35] version 2016/6.

The SQUEEZE procedure as implemented in the PLATON program package[36] was applied to eliminate the structure factor contributions from partially occupied or spatially disordered solvent molecules in the crystal structures using a rolling ball algorithm with a radius of 1.2 Å to map the solvent accessible voids. In **1**, the volume containing disordered solvent in the unit cell was calculated to be 9260 Å^3 with 2001 electrons (corresponding to ~3 non-localized molecules DMF per formula unit). Note that these values do not include the solvent molecules localized during structure determination. For **2** and **3** the corresponding values are 678 Å^3 with 158 electrons (corresponding to ~2 non-localized molecules DMF per formula unit) and 8800 Å^3 with 2097 electrons (corresponding to ~6.5 non-localized molecules DMF per formula unit), respectively.

Crystal data as well as details of data collection and refinement for **1–3** are summarized in Table 1. Topological analysis was performed using ToposPro package. ToposPro TTD and TTO collections were used for the search of topologies and their occurrences.[37]

Table 1. Crystallographic data for **1-3**.

Compound	**1**	**2**	**3**
Empirical formula	$C_{48}H_{38}N_2O_{14}P_2Zn_3$	$C_{62}H_{40}N_4O_{12}P_2Zn_3$	$C_{52}H_{32}N_2O_{12}P_2Zn_3$
Formula weight	1124.85	1291.03	1134.84
Temperature / K	250(2)	100(2)	103(2)
Crystal system, space group	Tetragonal, $I4_1/acd$	Monoclinic, $P2/n$	Orthorhombic, *Ibca*
Radiation type	Synchrotron, λ = 0.69563 Å	Mo *K*α, λ = 0.71073 Å	Mo *K*α, λ = 0.71073 Å
a, *b*, *c* / Å	24.9279(6), 24.9279(6), 41.3855(17)	19.8106(7), 8.2214(3), 21.8115(8)	25.986 (3), 23.633 (2), 26.746 (3)
α, β, γ / °	90, 90, 90	90, 111.777(1), 90	90, 90, 90
V / Å^3	25717.0(16)	3298.9(2)	16425 (3)
Z	16	2	8
Calculated density / Mg·m^{-3}	1.162	1.300	0.918
Absorption coefficient / mm^{-1}	1.141	1.189	0.947
F(000)	9152	1312	4592
Crystal size / mm	0.1 x 0.1 x 0.1	0.254 x 0.115 x 0.035	0.642 x 0.598 x 0.138
Crystal colour, habit	Colourless, Prism	Colourless, Elongated plate	Colourless, Irregular plate
Theta range for data collection / °	1.485 to 20.347	2.011 to 25.040	1.917 to 25.346

Index ranges	-24<=h<=24, -24<=k<=24, -41<=l<=35	-23<=h<=23, -9<=k<=9, -25<=l<=25	-31<=h<=31, -28<=k<=28, -32<=l<=32
Reflections collected	35722	36736	91626
Independent reflections	3373 [R(int) = 0.1350]	5848 [R(int) = 0.0699]	7537 [R(int) = 0.0609]
Absorption correction	Semi-empirical from equivalents	Numerical	Semi-empirical from equivalents
Refinement method	Full-matrix least-squares on F^2	Full-matrix least-squares on F^2	Full-matrix least-squares on F^2
Data, restraints, parameters	3373, 24, 314	5848, 98, 418	7537, 276, 321
Goodness-of-fit on F^2	1.032	1.045	1.137
Final R indices [I>2sigma(I)]	R1 = 0.0472, wR2 = 0.1019	R1 = 0.0437, wR2 = 0.1120	R1 = 0.0491, wR2 = 0.1410
R indices (all data)	R1 = 0.0778, wR2 = 0.1137	R1 = 0.0579, wR2 = 0.1199	R1 = 0.0647, wR2 = 0.1578
Largest diff. peak and hole / e·Å^{-3}	0.246 and -0.283	0.743 and -0.724	0.574 and -0.503

Powder X-ray diffraction. Powder X-ray diffraction was carried out on a Bruker AXS D8 Advance diffractometer equipped with an automatic multisampler. Data collection was performed using monochromatic Cu $K\alpha_1$ radiation in Bragg-Brentano geometry. A flat sample holder with glass surface was used for the measurements. Powder X-ray diffraction for **3** was additionally carried out on a high resolution diffractometer with Debye-Scherrer geometry in glass capillaries of 1 mm diameter using synchrotron radiation (BM31) at the Swiss-Norwegian Beamlines at the ESRF. Pawley profile fits for powder X-ray diffraction data were calculated using TOPAS 4.2.

Thermal analysis. A Netzsch STA 449 F1 Jupiter was used for simultaneous thermogravimetric-differential scanning calorimetry measurements in a flow of Ar and a heating rate of 2 K min^{-1}.

Gas adsorption. Gas adsorption measurements were carried out on a BELSORP-max instrument. Samples were pre-treated by immersion in deaerated $CHCl_3$ (**1**) or CH_2Cl_2 (**2** and **3**) for 3-5 times, subsequent separation of the solid by filtration and heating the resulting material in a dynamic vacuum at 338 K (**1**) or 298 K (**2** and **3**) overnight. Samples were transferred into the glove box, where sample cells were filled and transferred to the instrument under inert atmosphere using quick seals. Prior to the sorption experiment, the samples were heated once more in a dynamic vacuum at 338 K (**1**) or 298 K (**2** and **3**).

RESULTS AND DISCUSSION

Single Crystal Structures

*Structure of **1***

$[Zn_3(tpp)_2 \cdot (DMF)_2] \cdot n$DMF (**1**) crystallizes in tetragonal space group $I4_1/acd$. The inorganic secondary building unit is a trinuclear Zn cluster (Figure 1a). The Zn1 atom at the center of the unit is situated on a special position. It has a distorted octahedral coordination environment formed by oxygen atoms of the carboxylate group from different tpp^{3-} ligands. The two equivalent terminal Zn2 atoms in the SBU are located on a general position and have a distorted tetrahedral coordination environment. Three of the coordinating oxygen atoms belong to carboxylate groups from the tpp^{3-} anion and the fourth is the oxygen atom of a coordinating DMF solvent molecule. Zn1 and Zn2 atoms are connected through two bridging carboxylate groups and one μ-bridging oxygen atom from another carboxylate group. In total, the trinuclear zinc SBU is coordinated by carboxylate groups from 6 different tpp^{3-} anions.

The organic linker and the inorganic SBUs form a two-dimensional layer (Figure 1b). It is described in a standard cluster representation as 3,6-c net with stoichiometry of $(3\text{-c})_2(6\text{-c})$, where the inorganic SBU is considered as 6-coordinate node and the organic linker is represented as 3-coordinate node (Figure 1c). The 3,6-connected two-dimensional net has $(4^3)_2(4^6\cdot6^6\cdot8^3)$ point symbol and rather frequently encountered **kgd** type topology.[37] For example, the same topology was observed for other coordination networks based on similar trinuclear zinc SBUs and tritopic linkers with terminal carboxylate groups, such as 4',4''',4''''-nitrilotris(([1,1'-biphenyl]-4-carboxylic acid))[38] and 4,4′,4″-(2,4,6-triethylbenzene-1,3,5-triyl)tribenzoic acid.[39] The same topology occurs also for networks built using analogous trinuclear metal clusters based on other transition metals, including Co,[40-41] Cd and Mn.[41] There are also structures with trinuclear inorganic SBUs and tritopic linkers with different topologies.[40, 42-44]

The layers in **1** are stacked on top of each other in ABCDABCD fashion where the relationship between layers is described by the 4_1 screw axis along the *c* axis. The layers itself contain solvent accessible space, and coordinated DMF guest molecules from one layer are penetrating into the pores of the adjacent layer in the resulting 3-dimensional structure (Figure 1d).

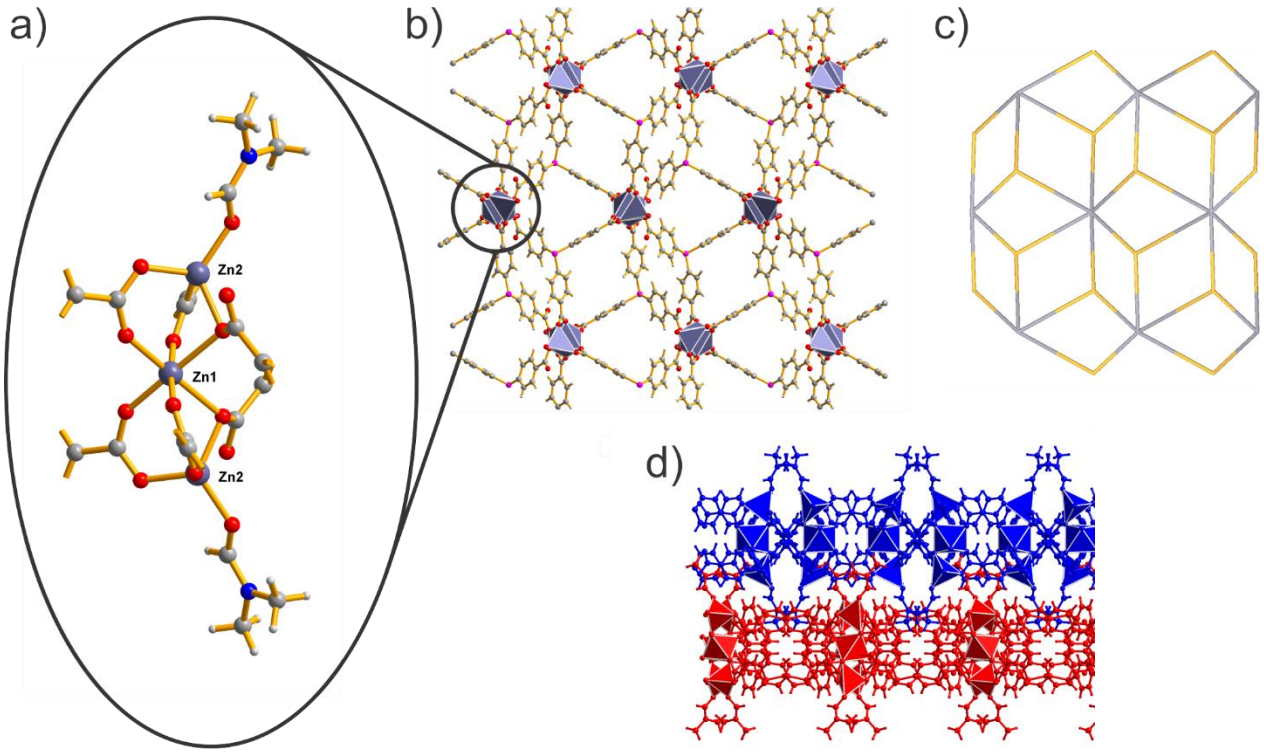

Figure 1. Crystal structure of **1**. a) Coordination environment of the trinuclear zinc SBU, b) View of the layer along [001] (coordinated DMF molecules are omitted for clarity), c) Schematic representation of the layer viewed along [001] illustrating the (3,6)-connected net with **kgd** topology, d) View along [010] (different adjacent layers are identified by blue and red).

In addition to DMF coordinated to Zn2, there are disordered DMF guest molecules occupying the pores and volume between the layers. The total pore volume calculated with PLATON[36] for the crystal structure with all DMF molecules subtracted from the structure is 12579.3 Å^3 (48.9 %) of the unit cell volume.

Thermal analysis of **1** in Ar flow (Figure 2a) showed gradual weight loss of 25 % by 533 K, corresponding to the loss of ~4.5 molecules of DMF per formula unit. There is no clear distinction in the weight loss trace between the removal of the coordinated and non-coordinated DMF guest molecules. The framework decomposes above 673 K.

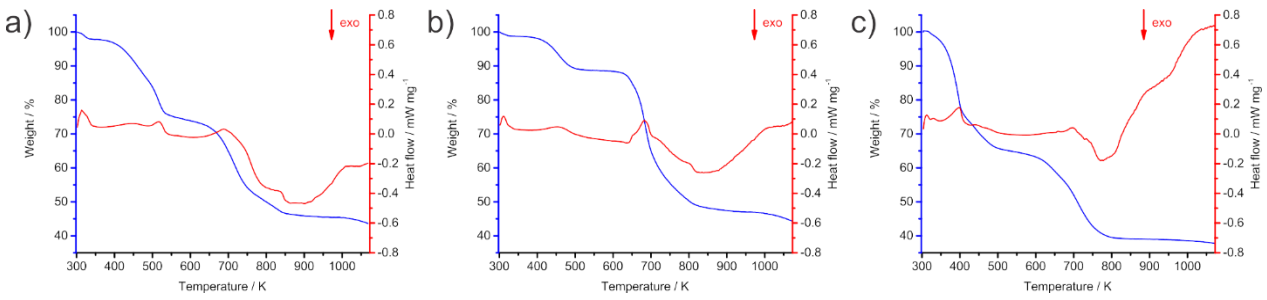

Figure 2. Simultaneous thermogravimetric analysis (blue) and differential scanning calorimetry (red) of a) **1**, b) **2**, c) **3**.

*Structure of **2***

An attempt to replace the coordinated DMF molecule in the trinuclear zinc SBU in **1** with neutral N-donor bridging linkers and incorporate these bridging linkers as spacers between adjacent layers was performed in order to increase the dimensionality of the framework. The one-pot synthesis with 4,4'-bipyridine as N donor ligand resulted in formation of $[Zn_3(tpp)_2(4,4'\text{-bipy})_2]\cdot n$DMF (**2**).

The crystal structure of **2** contains two different inorganic structural building units in the network. One is a Zn paddle wheel unit formed from four carboxylate groups from different tpp^{3-} linkers and two Zn1 atoms. The paddle wheel unit is coordinated by 4,4'-bipy linker molecules in the axial positions. The second framework node is an isolated Zn2 atom with distorted tetrahedral coordination environment of two oxygen and two nitrogen atoms. The two oxygen atoms around the zinc belong to carboxylate groups and the two nitrogen atoms are part of 4,4'-bipy molecules. The paddle wheel units ($\{Zn1\}_2$) and the Zn2 units are connected through the 4,4'-bipy linker and form infinite zig-zag chains $[-(\{Zn1\}_2)-(4,4'\text{-bipy})-Zn2\text{-}(4,4'\text{-bipy})-]_n$ (Figure 3a). Each tpp^{3-} linker is coordinated to one Zn2 atom and two ($\{Zn1\}_2$) units, thereby interconnecting 3 different zig-zag chains into a three-dimensional framework (Figure 3b).

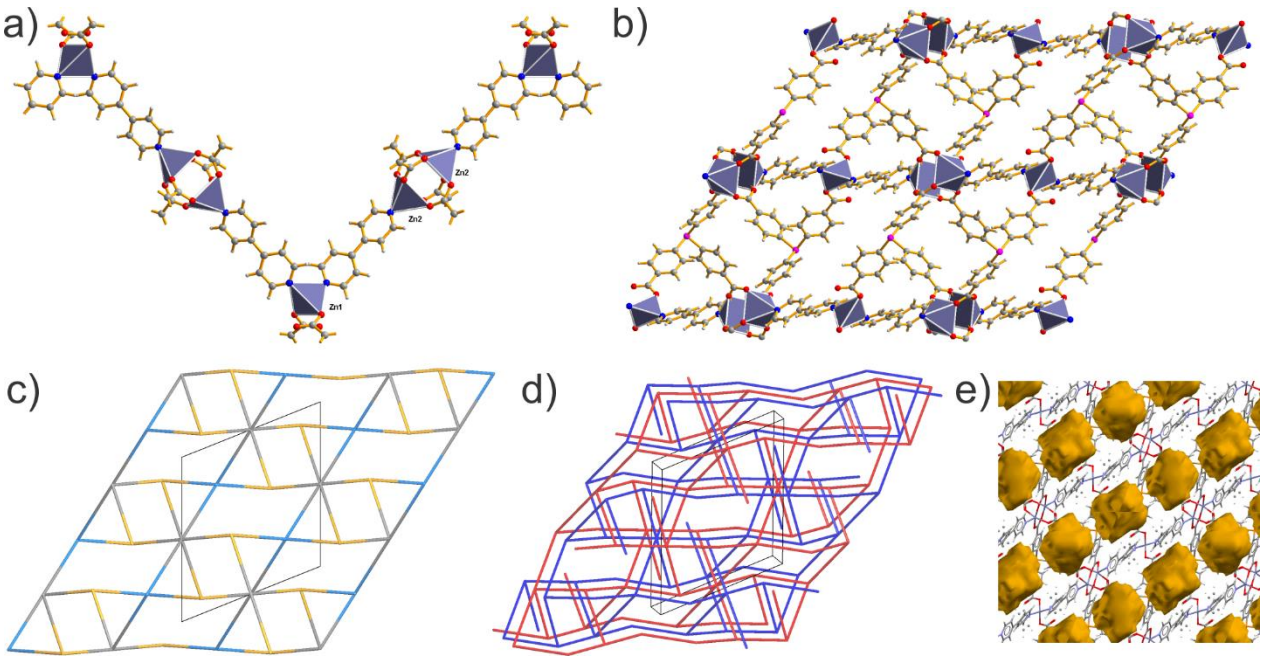

Figure 3. Crystal structure of **2**. a) Coordination environment of Zn atoms and the zig-zag chain formed from the Zn-containing structural building units and the neutral 4,4'-bipy ligands, b) The three-dimensional framework $[Zn_3(tpp)_2(4,4'\text{-bipy})_2]_n$, shown without interpenetration, c) Schematic representation of the (3,4,6)-connected non-interpenetrated net, viewed along [010], d) Schematic representation of the two interpenetrating nets (in blue and red, respectively), e) Illustration of the solvent filled cavities in the interpenetrated structure (calculated with Mercury).

The combination of both double N-capped paddle wheel and single metal center with two N-donors and two oxygen atoms in tetrahedral coordination environment in one structure is rare in coordination polymers. For instance, a combination of paddle wheel SBU based on Cu and tetrahedral metal SBU (Cu[45-48] or Ag[49]) in one structure resulted in formation of 1D coordination chains, while $[Zn_4(H_2O)(ip)_4(py)_6]_n$ (H_2ip = isophthalic acid and py = pyridine) is a two-dimensional layered network with paddle wheel and tetrahedral metal SBUs formed from Zn.[50] To the best of our knowledge, compound **2** is the first example of a 3D MOF possessing these structural features.

The three-dimensional network of **2** is represented as a 3,4,6-c, 3-nodal net with $(3\text{-c})_2(4\text{-c})(6\text{-c})$ stoichiometry, with the organic linker as 3-coordinate node, Zn2 as 4-coordinate node and the ($\{Zn1\}_2$) paddle wheel as 6-coordinate node (Figure 3c). The network has $(5^2\cdot6^4)(5^2\cdot6)_2(5^4\cdot6^6\cdot7^2\cdot8\cdot9^2)$ point symbol and a rare type of topology with the identifier **3,4,6T72** in the ToposPro TTD collection.[37] According to the ToposPro TTO collection,[37] only a few examples of networks of this topology are known. To the best of our knowledge, there are only five occurrences of this topology in coordination polymers in the standard cluster representation.[51-55]

The crystal structure of **2** is formed from two equivalent interpenetrating nets. The nets are related to each other by translation by one unit cell in [010] direction (Figure 3d). This type of interpenetration is classified as Ia and is a frequent type of interpenetration in MOFs.[56]

The solvent occupied volume of the unit cell amounts to 678.5 $Å^3$ (20.6 %), calculated with PLATON. The void space is located in the form of isolated zero-dimensional pores in the crystal structure (Figure 3e). There are four such cavities per unit cell, two with a volume of 160 $Å^3$ and two with a volume of 179 $Å^3$, respectively. Disordered DMF molecules are trapped in the cavities. The P(III) atom of the organic linker points towards the pore with its free electron pair. It is not involved in any significant interaction, such as coordination.

Thermal analysis of **2** in Ar flow (Figure 2b) shows a weight loss of 11 % and an endothermic peak at about 453 K that corresponds to the loss of ~2 molecules of DMF per formula unit. In the range of 493–633 K a plateau is observed in the weight plot, followed by a sharp decrease of the weight above 633 K. Compound **2** shows the most pronounced plateau of the three materials. Usually, this is an indication that it might be possible to obtain the desolvated framework structure. However, in the case of **2**, it is clear that major rearrangement of the structure must occur to allow the solvent molecules in the 0D pores to pass. Indeed, the long range order of **2** was lost on attempt

to remove the DMF from the pores by heating in vacuum overnight at 473 K (the temperature at which the plateau begins).

*Structure of **3***

The addition of 3,3'-bipyridine as N-donor ligand in a one-pot synthesis resulted in the formation of $[Zn_3(tpp)_2(3,3'\text{-bipy})]\cdot n$DMF (**3**). The inorganic secondary building unit is the same trinuclear zinc SBU as in **1** with one octahedrally coordinated Zn1 atom in the center and two tetrahedrally coordinated terminal Zn2 atoms (Figure 4a). The difference is that the O-coordinated DMF molecules in **1** are replaced in **3** with N-coordinated 3,3'-bipyridine, as intended by our alteration of the synthetic procedure. The trinuclear zinc SBUs and the phosphine linker form layers with identical connectivity as in **1**. The 3,3'-bipyridine ligand interconnects these layers into a 3D non-interpenetrated framework with solvent filled pores (Figure 4c). Minor conformational changes between the two layer structures are reflected in expansion of the *a* and compression of the *b* lattice parameter, which represent the plane in which the layer is located. **1** crystallizes in the tetragonal crystal system with $a = b = 24.9279(6)$ Å, while **3** crystallizes in the orthorhombic crystal system with $a = 25.986(3)$ and $b = 23.633(2)$ Å.

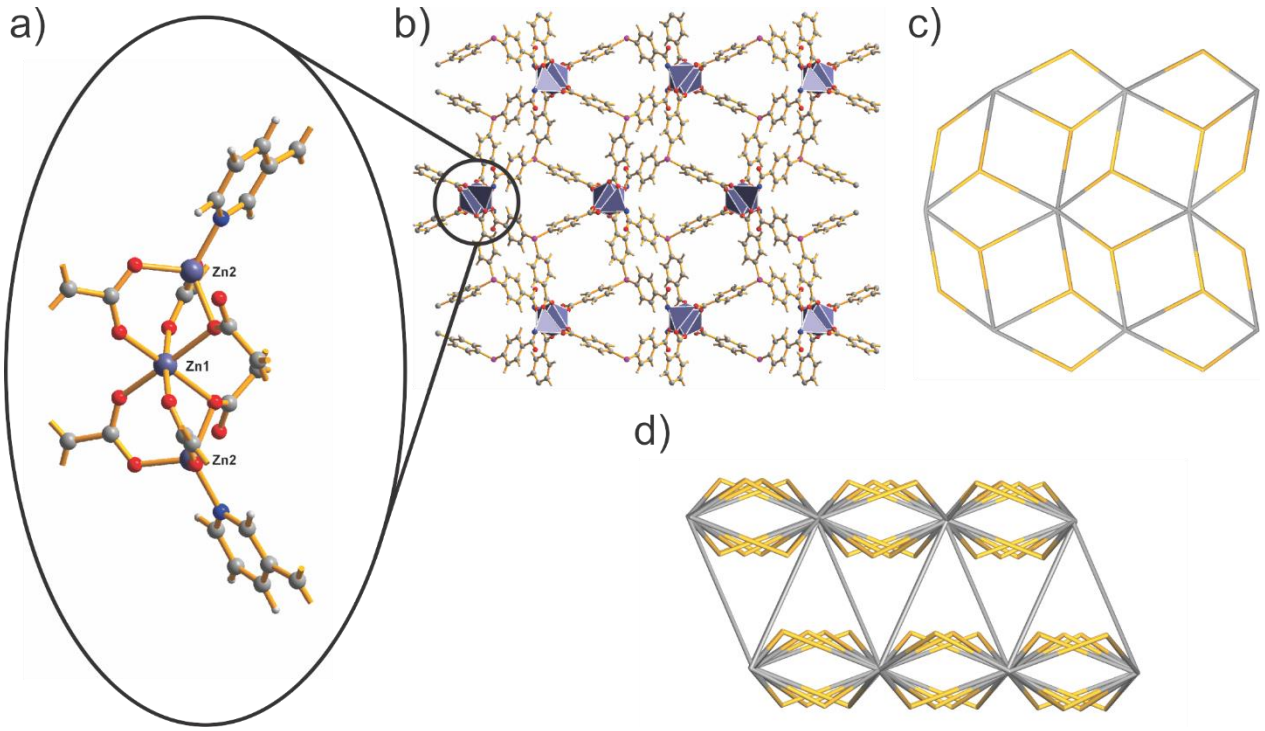

Figure 4. Crystal structure of **3**. a) Coordination environment of the trinuclear zinc SBU, b) View of the layer along [001] (coordinated pillar molecules are omitted for clarity), c) Schematic representation of a single layer (without taking into account the link to the next layer), viewed along [001], illustrating its (3,6)-connectivity and **kgd** topology, d) Schematic representation of the framework, illustrating the connection between the layers in the (3,8)-connected net.

The network can be simplified to a 3,8-c net with stoichiometry $(3\text{-c})_2(8\text{-c})$, where the 3-c node is tpp^{3-} and the 8-c node is the trinuclear zinc SBU. The network has point symbol $(4^3)_2(4^6\cdot6^{18}\cdot8^4)$ and the topology identifier **3,8T15** in the ToposPro TTD collection.[37] The **3,8T15** topology is not identical to the more frequently occurring **tfz-d** topology. The coordination sequences of these two topologies are different, even though they both have identical point symbols.[57,58] According to the ToposPro TTO collection,[37] the **3,8T15** topology is rather rare and has occurred only 4 times in coordination polymers in the standard cluster representation.[59-60] Structure **3** is the first example of compound with this topology with Zn as metal component.

Compound **3** contains a three-dimensional pores system. The total pore volume (calculated using PLATON) is 8793.2 $Å^3$ (53.5 %) per unit cell. Unfortunately, the potential coordination site of the phosphorus atom in the triphenyl phosphine linker is shielded from access from the pore space by a nearby 3,3'-bipyridine linker. As a consequence, it is not available for post-synthetic coordination of homogenous catalyst systems.

Thermal analysis of **3** in Ar flow showed a weight loss of 34 % in the range from 305–493 K, corresponding to the endothermic loss of ~8 molecules of DMF per formula unit. The weight loss above 633 K corresponds to the ultimate decomposition of the framework. The bulk of the weight loss connected to solvent removal occurred below 403 K for **3**, while it occurred in the range 433–473 K for **1** and **2**, indicating more facile transport of the solvent in the interconnected pore system of **3**.

Changes in the powder X-ray diffraction pattern are observed already upon drying of the material at 298 K (Figure S5). Initially, only changes in relative intensities are observed during the drying process, but no significant peak shifts. After some time, a sharp change of peak positions is observed, which means there is a major rearrangement of the framework structure. After the resolvation with DMF, the original powder X-ray diffraction pattern is restored, indicating that the transformation is reversible and related to the amount of solvent in the pore.

The approach of building MOFs with pillared-layered structures using N-donor bridging ligands has been successfully used for the synthesis of a variety of porous, so-called jungle-gym MOFs.[61-70] Among these are also pillared-layered MOF structures with (3,8)-connectivity, as in **3,** in which the layers formed from the inorganic SBU and the carboxylate-bearing organic linkers are pillared with linear N-donor bridges into three-dimensional networks.[38, 71-76]

There are only few reported cases for which the layered (3,6)-connected and pillared-layered (3,8)-connected metal-organic frameworks are built from identical layers, as in **1** and **3**

respectively. To the best of our knowledge, the only examples are the layered $[Co_4(OABDC)_2(OH)_2(H2O)_4]\cdot 4.4H_2O$ and pillared-layered $[Co_2(OABDC)(bpe)(OH)]\cdot 2.9H_2O$ (OABDC = 5-oxyacetateisophthalate, bpe = 1,2-bis(4-pyridyl)ethylene)[77]. Like in **1**, $[Co_4(OABDC)_2(OH)_2(H2O)_4]\cdot 4.4H_2O$ contains a 2D network of **kgd** topology. The addition of bpe as a pillar to the one-pot synthesis then resulted in a formation of (3,8)-connected pillared-layered structure $[Co_2(OABDC)(bpe)(OH)]\cdot 2.9H_2O$ with **tfz-d** topology. This is very much in analogy to the formation of **1** and **3**, respectively, which depended on the absence or addition of 3,3'-bipyridine to the reaction mixture.

Gas sorption

The crystal structures of compounds **1-3** revealed the presence of solvent filled pores and with these the potential for permanent porosity. We exchanged the high-boiling DMF guest solvent molecules with $CHCl_3/CH_2Cl_2$ and subsequently treated the materials in a dynamic vacuum in an attempt to remove the solvent from the pores and investigate the porosity of the compounds.

The exchange of the solvent in **1** with $CHCl_3$ resulted in significant shift of peaks in the powder X-Ray diffraction pattern and simultaneous decrease of the long-range order of the structure (Figure S2). As-synthesized **1** contains coordinated DMF molecules at the trinuclear zinc moiety that penetrate into adjacent layers and contribute to the ordering of the layers. When these are removed, the layers can shift in respect to each other and diminish the long-range order in the process. After treating the sample in a dynamic vacuum at 338 K overnight, the material had lost almost all crystallinity (Figure S2). Despite the loss of long-range order, the desolvated material adsorbed CO_2 at 195 K (Figure 5). The loss of long-range order upon removal of the guest solvent molecules is typical for layered MOF structures. Even though, the resulting amorphous material can still show selective gas sorption.[78]

The pores in the crystal structure of **2** are isolated, at least in a static picture of the structure. Thus, they should not permit the diffusion of guest molecules, which seems to be confirmed by the absence of N_2 adsorption at 77 K (Figure 5). However, the material actually does display CO_2 sorption at 195 K. A sample of **2** was soaked in CH_2Cl_2 overnight and then treated in a dynamic vacuum at 298 K. The material remained crystalline and there were no significant peak shifts observed in comparison to the pattern of the as-synthesized compound (Figure S3). Substance pre-treated in this way exhibited adsorption of CO_2 at 195 K, but it did not adsorb N_2 at 77 K (Figure 5). We ascribe the access of CO_2 to the 0D pores in the single crystal structure to the rotational freedom of the phenyl rings and the faster kinetics at the higher temperature of 195 K than 77 K. A change of dihedral angle between phenyl ring and the carboxylate groups coordinating the inorganic metal centers might open up a pathway that allows the transport of molecules in and out of the cavities. The rotation of phenyl rings has been established in MOF-5,[79] MIL-53/47[80] and other MOFs using NMR measurements. It can be anticipated that the same effect takes place in **2** for all or selected phenyl rings in dependence of steric hindrance by the surrounding structural elements. In fact, one of the phenyl rings in the 4,4'-bipyridine linker is already disordered between two positions in the crystal structure measured at 100 K. The phenyl rings will most likely have even more rotational freedom at higher temperatures. A similar effect has been observed for CO_2 adsorption in $[Co(HL^{dc})]\cdot 1.5MeOH\cdot dioxane$[81] ($[HL^{dc}]^{2-}$ = 4'-(3'-carboxy-[4,2':6',4''-terpyridin]-4'-yl)-[1,1'-biphenyl]-3,5-dicarboxylate), in which the rotation of phenyl rings resulted in the transition between a narrow pore form and a large pore form and accordingly different amounts of CO_2 adsorption. A temperature dependence of the conformational changes allowing transport of the guest molecules explains the absence of N_2 adsorption at 77 K in **2** (Figure 5), if the rotation of the phenyl ring was hindered sufficiently at this temperature. In fact, a simple adjustment of dihedral angles in a structural model based on the single crystal structure of **2** as the starting point

indicates that the isolated cavities might become linked into one-dimensional channels. A rotation of the phenyl rings of the tpp^{3-} linkers by 0-30° (Figure 6) results in such a change of the pore dimensionality from 0-dimensional to 1-dimensional (Figure 6). Calculations with PLATON for this hypothetical structural model indicate formation of a pore with a volume of 787.6Å^3 (23.9% of the unit cell volume), replacing the four isolated cavities in the single crystal structure of **2**. The resulting channels would allow the transport of the solvent and CO_2 molecules in and out of the framework and rationalize the observed sorption of CO_2. However, the rotation of the phenyl rings is greatly restricted due to the steric factors. The modelled structure has a number of short contacts with the distance of ~2.0 Å.

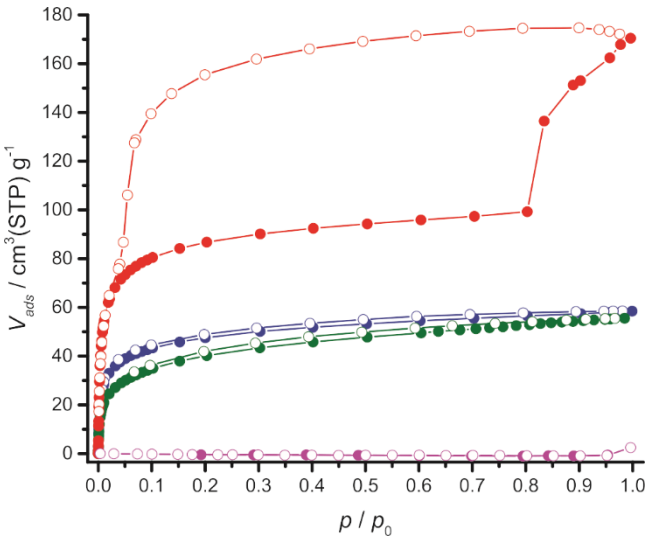

Figure 5. Carbon dioxide adsorption (closed symbols) and desorption (open symbols) isotherms at 195 K on **1** (blue), **2** (green) and **3** (red). Nitrogen adsorption (closed symbols) and desorption (open symbols) isotherms at 77 K on **2** (magenta) was measured after the carbon dioxide sorption experiments. In nitrogen sorption experiments at 77 K on **1** and **3** the equilibrium was not achieved in a reasonable time (only three data points at very low relative pressures had been recorded after 48 h), indicating that the kinetics of the sorption is very slow at this temperature.

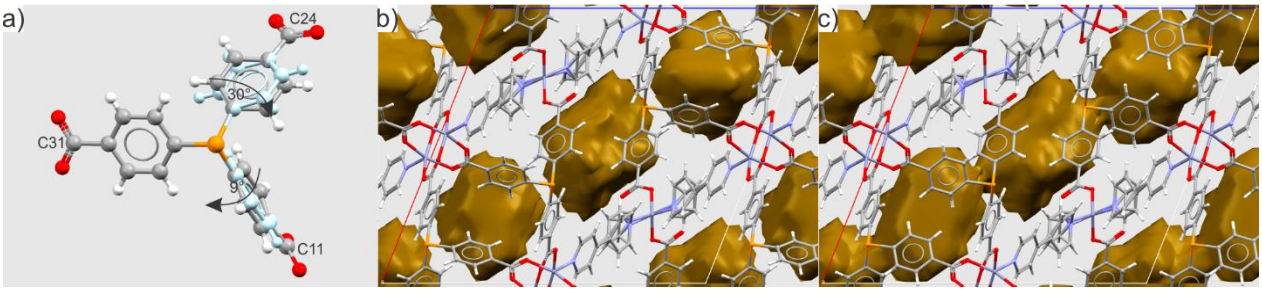

Figure 6. The modelling of the phenyl ring rotation. a) Hypothetical change of of the tpp^{3-} moiety in **2** as a result of rotation of phenyl rings,b) Isolated voids in **2** (calculated with Mercury), c) Channel-shaped voids for hypothetical structural model of **2** with rotated phenyl rings (calculated with Mercury).

In principle, the large interconnected net of pores in **3** is expected to allow facile diffusion of guest molecules. However, significant, reversible changes of the structure upon drying and removal of the guest solvent molecules of DMF were observed (Figure S5), indicating a pronounced flexibility of the structure in response to solvent content. This flexibility is reflected in the CO_2 sorption isotherms of **3**. The sample was pre-treated by solvent exchange with CH_2Cl_2 overnight and drying in dynamic vacuum at 298 K (Figure 5). A large gate opening effect was observed accounting for an increase in uptake of approx. 100 %. The gate opening occurred at $p/p_0 \sim 0.8$ on adsorption and gate closing occurred at $p/p_0 \sim 0.05$ on desorption, i.e. the gate effect showed a quite large hysteresis. The gate opening was shifted towards higher p/p_0 in consecutive adsorption cycles; in addition, the increase in uptake was significantly decreased by the third cycle (Figure S6). This means the structural rearrangement is not fully reversible and leads to a change in adsorption behavior over time.

CONCLUSION

Three new porous metal-organic frameworks containing P-sites in the structure were synthesized. N-donor bridging linkers were used successfully in the MOF synthesis together with H_3tpp, which led to the formation of the three-dimensional structures [Zn_3(tpp)$_2$(4,4'-bipy)$_2$] (**2**) and [Zn_3(tpp)$_2$(3,3'-bipy)] (**3**). The lone pair of the phosphorus atom in **2** points towards the pore space, but the fact that the pores are zero-dimensional restricts attempts of grafting transition metal catalyst systems onto the framework. However, the material showed CO_2 adsorption at 195 K, possibly due to rotational modes of the phenyl rings which allow the small CO_2 molecule to diffuse into the structure. The non-interpenetrated porous framework of **3** has a large interconnected net of pores. The structure shows flexibility in response to changes in the pore content and a large hysteresis in CO_2 sorption at 195 K. The pillaring approach employed for the synthesis of **3** might be broadened to a wider library of N-donor bridging linkers and extended triphenylphosphine based linkers,[21] in order to obtain stable porous MOFs with sufficiently large pore dimensions and P-sites available for grafting of homogeneous catalytic systems.

ASSOCIATED CONTENT

Supporting Information

Synthetic procedure of H_3tpp, powder X-ray diffraction data for **1-3** (Figures S1-S5), CO_2 sorption data for **3** (Figure S6), IR spectra for **1-3** (Figure S7), details on derivation of the hypothetical structural model of **2** (PDF).

Accession Codes

CCDC 1530215–1530217 contain the supplementary crystallographic data for this paper. These data can be obtained free of charge via www.ccdc.cam.ac.uk/data_request/cif, or by emailing

data_request@ccdc.cam.ac.uk, or by contacting The Cambridge Crystallographic Data Centre, 12 Union Road, Cambridge CB2 1EZ, UK; fax: +44 1223 336033.

AUTHOR INFORMATION

Corresponding Author

Pascal D. C. Dietzel, Department of Chemistry, University of Bergen, P.O. Box 7803, N-5020 Bergen, Norway, E-mail: pascal.dietzel@uib.no

Funding Sources

Research Council of Norway through grant ISP-KJEMI 209339 and SYNKNOYT 227702 and 247734.

ACKNOWLEDGMENT

We would like to thank Dr. Dmitry Chernyshov for kind assistance with the single crystal measurement at BM01 and Dr..Hermann Emerich for kind assistance with the powder X-ray diffraction measurement at BM31 at the Swiss-Norwegian Beamlines at the ESRF. This research was supported by the Research Council of Norway through grant ISP-KJEMI 209339 and SYNKNOYT 227702 and 247734.

ABBREVIATIONS

MOF, Metal-Organic Framework; SBU, secondary building unit; THF, tetrahydrofuran; DMF, dimethylformamide; SNBL, Swiss-Norwegian Beamlines.

REFERENCES

(1) Lammert, M.; Bernt, S.; Vermoortele, F.; De Vos, D. E.; Stock, N., *Inorg. Chem.* **2013,** *52*, 8521-8528.

(2) Farrusseng, D.; Aguado, S.; Pinel, C., *Angew. Chem., Int. Ed.* **2009,** *48*, 7502-7513.

(3) Gascon, J.; Aktay, U.; Hernandez-Alonso, M. D.; van Klink, G. P. M.; Kapteijn, F., *J. Catal.* **2009,** *261*, 75-87.
(4) Canivet, J.; Aguado, S.; Schuurman, Y.; Farrusseng, D., *J. Am. Chem. Soc.* **2013,** *135*, 4195-4198.
(5) Ma, L.; Falkowski, J. M.; Abney, C.; Lin, W., *Nat. Chem.* **2010,** *2*, 838-846.
(6) Astruc, D., *Organometallic Chemistry and Catalysis*. Springer Berlin Heidelberg: 2007.
(7) Bernard, M.; Ford, W. T., *J. Org. Chem.* **1983,** *48*, 326-332.
(8) Jiang, M.; Yan, L.; Sun, X.; Lin, R.; Song, X.; Jiang, Z.; Ding, Y., *React. Kinet., Mech. Catal.* **2015,** *116*, 223-234.
(9) Jiang, X.; Zhao, W.; Wang, W.; Zhang, F.; Zhuang, X.; Han, S.; Feng, X., *Polym. Chem.* **2015,** *6*, 6351-6357.
(10) Fritsch, J.; Drache, F.; Nickerl, G.; Böhlmann, W.; Kaskel, S., *Microporous Mesoporous Mater.* **2013,** *172*, 167-173.
(11) Hausoul, P. J. C.; Eggenhuisen, T. M.; Nand, D.; Baldus, M.; Weckhuysen, B. M.; Gebbink, R.; Bruijnincx, P. C. A., *Catal. Sci. Technol.* **2013,** *3*, 2571-2579.
(12) Hausoul, P. J. C.; Broicher, C.; Vegliante, R.; Gob, C.; Palkovits, R., *Angew. Chem., Int. Ed.* **2016,** *55*, 5597-5601.
(13) Zhang, Q.; Yang, Y.; Zhang, S., *Chem. - Eur. J.* **2013,** *19*, 10024-10029.
(14) Bek, D.; Balcar, H.; Žilková, N.; Zukal, A.; Horáček, M.; Čejka, J., *ACS Catal.* **2011,** *1*, 709-718.
(15) Melis, K.; De Vos, D.; Jacobs, P.; Verpoort, F., *J. Mol. Catal. A: Chem.* **2001,** *169*, 47-56.
(16) Miyaji, T.; Onozawa, S.-y.; Fukaya, N.; Ueda, M.; Takagi, Y.; Sakakura, T.; Yasuda, H., *J. Organomet. Chem.* **2011,** *696*, 1565-1569.
(17) Humphrey, S. M.; Allan, P. K.; Oungoulian, S. E.; Ironside, M. S.; Wise, E. R., *Dalton Trans.* **2009**, 2298-2305.
(18) Nunez, A. J.; Shear, L. N.; Dahal, N.; Ibarra, I. A.; Yoon, J.; Hwang, Y. K.; Chang, J.-S.; Humphrey, S. M., *Chem. Commun.* **2011,** *47*, 11855-11857.
(19) Nuñez, A. J.; Chang, M. S.; Ibarra, I. A.; Humphrey, S. M., *Inorg. Chem.* **2013,** *53*, 282-288.
(20) Václavík, J.; Servalli, M.; Lothschütz, C.; Szlachetko, J.; Ranocchiari, M.; van Bokhoven, J. A., *ChemCatChem* **2013,** *5*, 692-696.
(21) Sawano, T.; Lin, Z.; Boures, D.; An, B.; Wang, C.; Lin, W., *J. Am. Chem. Soc.* **2016,** *138*, 9783-9786.
(22) Bohnsack, A. M.; Ibarra, I. A.; Bakhmutov, V. I.; Lynch, V. M.; Humphrey, S. M., *J. Am. Chem. Soc.* **2013,** *135*, 16038-16041.
(23) Falkowski, J. M.; Sawano, T.; Zhang, T.; Tsun, G.; Chen, Y.; Lockard, J. V.; Lin, W., *J. Am. Chem. Soc.* **2014,** *136*, 5213-5216.
(24) Goesten, M. G.; Sai Sankar Gupta, K. B.; Ramos-Fernandez, E. V.; Khajavi, H.; Gascon, J.; Kapteijn, F., *CrystEngComm* **2012,** *14*, 4109-4111.
(25) Morel, F. L.; Ranocchiari, M.; van Bokhoven, J. A., *Ind. Eng. Chem. Res.* **2014,** *53*, 9120-9127.
(26) Xu, X.; Rummelt, S. M.; Morel, F. L.; Ranocchiari, M.; van Bokhoven, J. A., *Chem. - Eur. J.* **2014,** *20*, 15467-15472.
(27) Amengual, R.; Genin, E.; Michelet, V.; Savignac, M.; Genêt, J.-P., *Adv. Synth. Catal.* **2002,** *344*, 393-398.
(28) Dyadkin, V.; Pattison, P.; Dmitriev, V.; Chernyshov, D., *J. Synchrotron Radiat.* **2016,** *23*, 825-829.

(29) Rigaku (2014). Rigaku Oxford Diffraction, CrysalisPro Software System. Version 1.171.37.34.
(30) APEX2, Version 2014.2011-2010; Bruker-AXS: Madison, Wisconsin, USA, 2014.
(31) SAINT, Version 7.68A; Bruker-AXS: Madison, Wisconsin, USA, 2010.
(32) Krause, L.; Herbst-Irmer, R.; Sheldrick, G. M.; Stalke, D., *J. Appl. Crystallogr.* **2015,** *48*, 3-10.
(33) Sheldrick,G.,M., SHELXS-86 version 2013/1, *Acta Crystallogr., Sect. A* **2008,** *64*, 112–122.
(34) Sheldrick, G., M, *Acta Crystallogr., Sect. A* **2015,** *71*, 3-8.
(35) Sheldrick, G., M, *Acta Crystallogr., Sect. C* **2015,** *71*, 3-8.
(36) Spek, A., *Acta Crystallogr., Sect. D* **2009,** *65*, 148-155.
(37) Blatov, V. A.; Shevchenko, A. P.; Proserpio, D. M., *Cryst. Growth Des.* **2014,** *14*, 3576-3586.
(38) He, Y.-P.; Tan, Y.-X.; Zhang, J., *Chem. Commun.* **2013,** *49*, 11323-11325.
(39) King, S. C.; Lin, R.-B.; Wang, H.; Arman, H. D.; Chen, B., *Mater. Chem. Front.* **2017**.
(40) Kim, D.; Song, X.; Yoon, J. H.; Lah, M. S., *Cryst. Growth Des.* **2012,** *12*, 4186-4193.
(41) Lin, X.-M.; Niu, J.-L.; Chen, D.-N.; Lu, Y.-N.; Zhang, G.; Cai, Y.-P., *CrystEngComm* **2016,** *18*, 6841-6848.
(42) Wollmann, P.; Leistner, M.; Stoeck, U.; Grunker, R.; Gedrich, K.; Klein, N.; Throl, O.; Grahlert, W.; Senkovska, I.; Dreisbach, F.; Kaskel, S., *Chem. Commun.* **2011,** *47*, 5151-5153.
(43) Gedrich, K.; Heitbaum, M.; Notzon, A.; Senkovska, I.; Fröhlich, R.; Getzschmann, J.; Mueller, U.; Glorius, F.; Kaskel, S., *Chem. - Eur. J.* **2011,** *17*, 2099-2106.
(44) Han, L.; Qin, L.; Xu, L.-P.; Zhao, W.-N., *Inorg. Chem.* **2013,** *52*, 1667-1669.
(45) Luan, X.-J.; Cai, X.-H.; Wang, Y.-Y.; Li, D.-S.; Wang, C.-J.; Liu, P.; Hu, H.-M.; Shi, Q.-Z.; Peng, S.-M., *Chem. - Eur. J.* **2006,** *12*, 6281-6289.
(46) Dobrzańska, L.; Lloyd, G. O.; Jacobs, T.; Rootman, I.; Oliver, C. L.; Bredenkamp, M. W.; Barbour, L. J., *J. Mol. Struct.* **2006,** *796*, 107-113.
(47) McIldowie, M. J.; Mocerino, M.; Ogden, M. I.; Skelton, B. W., *Tetrahedron* **2007,** *63*, 10817-10825.
(48) Kraft, P. E.; LaDuca, R. L., *Acta Crystallogr., Sect. E* **2012,** *68*, m1049-m1050.
(49) Schultheiss, N.; Barnes, C. L.; Bosch, E., *Cryst. Growth Des.* **2003,** *3*, 573-580.
(50) Zhou, D.-S.; Wang, F.-K.; Yang, S.-Y.; Xie, Z.-X.; Huang, R.-B., *CrystEngComm* **2009,** *11*, 2548-2554.
(51) Yang, H.; Zhang, H.-X.; Hou, D.-C.; Li, T.-H.; Zhang, J., *CrystEngComm* **2012,** *14*, 8684-8688.
(52) Yang, W.; Wang, C.; Ma, Q.; Liu, C.; Wang, H.; Jiang, J., *CrystEngComm* **2014,** *16*, 4554-4561.
(53) Wen, Y.-H.; Zhang, Q.-W.; He, Y.-H.; Feng, Y.-L., *Inorg. Chem. Commun.* **2007,** *10*, 543-546.
(54) Rong-Yi Huang, H.-M. X., Kun Zhu, Guang-Xiang Liu, Xiao-Ming Ren,, *Chin.J.Struct.Chem.* **2009**, 1661.
(55) Zhao, L.; Zhao, C.; Guo, H.; Bai, H.; Zhang, M.; Chen, R., *Inorg. Chim. Acta* **2016,** *450*, 12-22.
(56) Baburin, I. A.; Blatov, V. A.; Carlucci, L.; Ciani, G.; Proserpio, D. M., *J. Solid State Chem.* **2005,** *178*, 2452-2474.
(57) Ohrstrom, L., *Crystals* **2015,** *5*, 154-162.

(58) Coordination sequences for **tfz-d** are '3 18 41 74 113 164 221 290 365 452', dt10=1741 and '8 20 44 74 116 164 224 290 368 452', dt10=1760; while for **3,8T15** are '3 18 43 80 135 192 261 350 439 542', dt10=2063 and '8 20 48 90 136 196 272 350 444 552', dt10=2116.
(59) Luo, F.; Che, Y.; Zheng, J., *Cryst. Growth Des.* **2008,** *8*, 2006-2010.
(60) Zhou, J.; Yan, S.; Yuan, D.; Zheng, X.; Li, L.; Jin, L., *CrystEngComm* **2009,** *11*, 2640-2649.
(61) Dybtsev, D. N.; Chun, H.; Kim, K., *Angew. Chem., Int. Ed.* **2004,** *43*, 5033-5036.
(62) Dybtsev, D. N.; Yutkin, M. P.; Peresypkina, E. V.; Virovets, A. V.; Serre, C.; Férey, G.; Fedin, V. P., *Inorg. Chem.* **2007,** *46*, 6843-6845.
(63) Chun, H.; Dybtsev, D. N.; Kim, H.; Kim, K., *Chem. - Eur. J.* **2005,** *11*, 3521-3529.
(64) Seki, K., *Chem. Commun.* **2001**, 1496-1497.
(65) Wang, H.; Getzschmann, J.; Senkovska, I.; Kaskel, S., *Microporous Mesoporous Mater.* **2008,** *116*, 653-657.
(66) Seki, K.; Mori, W., *J. Phys. Chem. B,* **2002,** *106*, 1380-1385.
(67) Kondo, M.; Okubo, T.; Asami, A.; Noro, S.-i.; Yoshitomi, T.; Kitagawa, S.; Ishii, T.; Matsuzaka, H.; Seki, K., *Angew. Chem., Int. Ed.* **1999,** *38*, 140-143.
(68) De, D.; Neogi, S.; Bharadwaj, P. K., *Cryst. Growth Des.* **2016,** *16*, 5238-5246.
(69) Kitaura, R.; Iwahori, F.; Matsuda, R.; Kitagawa, S.; Kubota, Y.; Takata, M.; Kobayashi, T. C., *Inorg. Chem.* **2004,** *43*, 6522-6524.
(70) Uemura, K.; Yamasaki, Y.; Komagawa, Y.; Tanaka, K.; Kita, H., *Angew. Chem., Int. Ed.* **2007,** *46*, 6662-6665.
(71) Dong, X.-Y.; Si, C.-D.; Fan, Y.; Hu, D.-C.; Yao, X.-Q.; Yang, Y.-X.; Liu, J.-C., *Cryst. Growth Des.* **2016,** *16*, 2062-2073.
(72) Chen, S.-S.; Zhao, Y.; Fan, J.; Okamura, T.-a.; Bai, Z.-S.; Chen, Z.-H.; Sun, W.-Y., *CrystEngComm* **2012,** *14*, 3564-3576.
(73) Zhang, X.; Ma, G.; Kong, F.; Yu, Z.; Wang, R., *Inorg. Chem. Commun.* **2012,** *22*, 44-47.
(74) He, K.-H.; Li, Y.-W.; Chen, Y.-Q.; Song, W.-C.; Bu, X.-H., *Cryst. Growth Des.* **2012,** *12*, 2730-2735.
(75) Song, X.-Z.; Song, S.-Y.; Zhu, M.; Hao, Z.-M.; Meng, X.; Zhao, S.-N.; Zhang, H.-J., *Dalton Trans.* **2013,** *42*, 13231-13240.
(76) Peng, Y.-F.; Zhao, S.; Li, K.; Liu, L.; Li, B.-L.; Wu, B., *CrystEngComm* **2015,** *17*, 2544-2552.
(77) Wang, G.-H.; Lei, Y.-Q.; Wang, N.; He, R.-L.; Jia, H.-Q.; Hu, N.-H.; Xu, J.-W., *Cryst. Growth Des.* **2010,** *10*, 534-540.
(78) Matoga, D.; Gil, B.; Nitek, W.; Todd, A. D.; Bielawski, C. W., *CrystEngComm* **2014,** *16*, 4959-4962.
(79) Gonzalez, J.; Nandini Devi, R.; Tunstall, D. P.; Cox, P. A.; Wright, P. A., *Microporous Mesoporous Mater.* **2005,** *84*, 97-104.
(80) Kolokolov, D. I.; Jobic, H.; Stepanov, A. G.; Guillerm, V.; Devic, T.; Serre, C.; Ferey, G., *Angew. Chem., Int. Ed.* **2010,** *49*, 4791-4794.
(81) Yang, W.; Davies, A. J.; Lin, X.; Suyetin, M.; Matsuda, R.; Blake, A. J.; Wilson, C.; Lewis, W.; Parker, J. E.; Tang, C. C.; George, M. W.; Hubberstey, P.; Kitagawa, S.; Sakamoto, H.; Bichoutskaia, E.; Champness, N. R.; Yang, S.; Schroder, M., *Chem. Sci.* **2012,** *3*, 2993-2999.

For Table of Content use only

Modification of Network and Pore Dimensionality in Metal-Organic Frameworks Containing a Secondary Phosphine Functionality

*Andrey A. Bezrukov, Karl W. Törnroos and Pascal D. C. Dietzel**

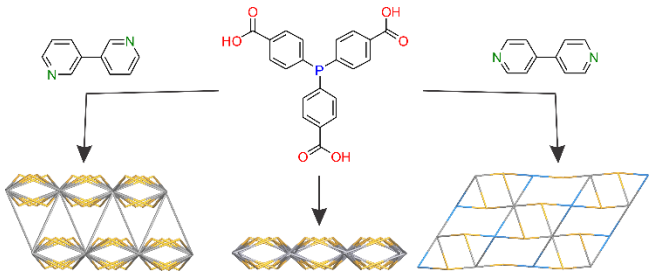

Three porous metal-organic frameworks were synthesized using a tridentate triphenylphosphine derivative as organic linker. The addition of N-donor linkers directed the synthesis between layered and three-dimensional frameworks with different rare topologies. All three compounds exhibit CO_2 adsorption at 195 K, including the occurrence of a large gate opening effect for one of them.